APPLICATION OF THE QUANTUM ESPRESSO CODE TO STUDY THE STRUCTURAL AND ELECTRONIC PROPERTIES OF TITANIUM DIOXIDE: A DFT STUDY

By

ESEKON JAMES IKAI

I56/75229/2014

A PROJECT SUBMITTED IN PARTIAL FULFILMENT OF THE REQUIREMENTS FOR THE DEGREE OF MASTER OF SCIENCE IN PHYSICS OF UNIVERSITY OF NAIROBI, KENYA.

MAY, 2016

DECLARATION

I, Esekon James Ikai, hereby declare that this project is my own original work, and it has not been presented for any degree to any institution of higher learning. Further, I declare that no part of this project may be reproduced without my prior permission and/or the University of Nairobi.

Esekon James Ikai

Signature: ..... Date: .....

I56/75229/2014

Declaration by Supervisors

The University of Nairobi Supervisors approve this project for examination.

Signature: ..... Date: .....

Dr. Musembi Juma Robinson,

Department of Physics,

University of Nairobi, Kenya.

Signature: ..... Date: .....

Dr. Wamalwa Dismas Simiyu,

Department of Physics,

University of Nairobi, Kenya.

DEDICATION

The project is a dedication to my family and all my friends.

ABSTRACT

Titanium dioxide attracts great attention as a wide band gap transition metal oxide due to its n-type semiconducting property which makes it to have many applications in industry, an area that has not been fully investigated. This study therefore focuses on the investigation of the structural properties and electronic band structures of the two phases of TiO_2, the rutile and anatase using ab-$initio$ methods. The structural properties were obtained using generalized gradient approximation (GGA) employing pseudo-potentials and plane wave basis sets.

For the two TiO_2 phases the calculated equilibrium lattice constants, bulk moduli and bond lengths were found to agree with a number of other recent theoretical calculations and also with experimental findings. The electronic properties were also investigated. Perfect bulk rutile and anatase gave band gaps of 2.09 eV and 2.48 eV respectively under ground state conditions. Valence band width (VB) of 1.65 eV and conduction band with (CB) of 5.917 eV were observed for rutile, TiO_2 while VB of 3.98 eV and CB of 2.05 eV were observed for anatase TiO_2 all in agreement with experimental values.

TABLE OF CONTENTS

LIST OF FIGURES

LIST OF TABLES

List of Symbols and Abbreviations

The following are the symbols and acronyms used in this project.

arb. units	Arbitrary Units
B_o	Bulk modulus
BC	boundary conditions
BOA	Born-Oppenheimer approximation
BSE	Bathe-Salpeter Equation
BZ	Brilloune Zone
CASTEP	Cambridge Serial Total Energy Package
CB	conduction band
CBM	conduction band minimum
CHPC	Centre for High Performance Computing
CI	configuration interaction
CMSG	Computational Material Science Group
DFT	Density Functional Theory
DOS	Density of states
EAS	Electron absorption spectroscopy
Ecut	kinetic energy cut-off
Ecutrho	charge density cut-off
E_{tot}	Total Energy
EELS	electron energy loss spectroscopy
Exp. Value	Experimental Values
V_{xc}	Exchange Energy

GGA	Generalized Gradient Approximation
H-F	Hartree-Fock
H-K	Hohenberg-Kohn
$\hat{H}$	Hamiltonian operator
HOMO	Highest occupied molecular orbital
KE	Kinetic energy
K-S	Kohn-Sham
LAPW	Linear augmented plane waves
LCAO	linear combination of atomic orbital
LC	linear combination
LDA	Local Density Approximation
LSDA	Local Spin Density Approximation
LUMO	Lowest unoccupied molecular orbital
MBPT	many body perturbation theory
MD	Molecular dynamics
NACOSTI	National Council for Science, Technology and Innovations
NC-PP	Norm-conserving pseudo-potential
NIR	near infra-red
PAW	Projector augmented waves
PDOS	Projected density of states
PE	Potential energy
PP	Pseudo-potential

PW	plane wave
PWSCF	Plane wave self-consistent field
QE	Quantum ESPRESSO
QM	Quantum mechanics
QP	Quasi particle
RSPT	Rayleigh-Schroedinger Perturbation Theory
SC	self-consistent
TDDFT	Time Dependent Density Functional Theory
TMO	Transition metal oxide
TM	Transition metal
UV	Ultra-violet
VB	valence band
VBM	valence band maximum
VESTA	Visualization system for Electronic and Structural Analysis
V_{ex}	Exchange-correlation potential
XcrysDen	X-Window Crystalline Structure and Densities

ACKOWLEDGEMENT

Many thanks to the most high for His graces without which the completion of this project would not be possible. Special appreciation to my supervisors, Dr. Musembi Robinson and Dr. Wamalwa Simiyu for their expertise, dedication, drive and encouragement during this study.

Appreciation goes to the following institutions: The Kenya Government through the National Council for Science, Technology and Innovations (NACOSTI) for their financial support, Centre for High Performance Computing (CHPC), Capetown, Republic of South Africa, for the use of their HPC cluster facility and the University of Eldoret (U.o.E) for the use of their resources during this study.

I'm also indebted to my co-researchers in the Computational Material Science Group (CMSG), at the University of Eldoret ; Perpetua Muchiri, Caroline Bakasa, Denis Magero, Odede Arkipo Ogwe and especially Ngeywo Tolbert Kaner for his continued technical and moral support.

Special gratitude to Prof. Amollo George and Dr. Nicholas Makau all of University of Eldoret for their timely support and encouragement in this area of my study. God bless you so much.

CHAPTER ONE

INTRODUCTION

1.1 Background

Titanium dioxide attracts great attention as primary material in several applications including white pigment preparation, photocatalysis, dye sensitized solar cells and nanoscale electronic devices. The rutile phase of TiO_2 has the simple and best known structure. It easily yields to a perfect rutile matrix after sputtering and annealing by varying temperatures which directly determine the physical and chemical behaviour of TiO_2.

Transition metal oxides are some of the most difficult classes of solids on which to perform theoretical predictions using first principle calculations. This is due to their complex crystal structures and the fact that they usually exhibit a wide range of properties including insulating, semiconducting and super conducting, as well as being ferroelectric and magnetic materials. As a prototypical semiconducting transition metal oxide, TiO_2 is the focus of extensive theoretical and experimental studies for over four decades due to its numerous technological applications [6].

1.2 Titanium Dioxide Phases

Titanium dioxide crystallizes in many phases [18]. The three major phases are rutile, Anatase and Brookite. [7]. Out of the three major phases, only rutile and anatase are currently being used for various known applications, thus extensive studies both experimental and theoretical with interesting physical and chemical properties have been harnessed on the bulk structures and literature on both bulk and surfaces is available[10]. Rutile is the most thermodynamically stable except for the nanometer scale and possibly at very low temperatures for which anatase is known to be stable[15]. It is reported that at temperature between $400 - 1000^o c$, anatase transforms to rutile.

The two main structure phases of TiO_2 (rutile and anatase), are tetragonal structures characterized by two complementary $TiO_x O_y$ building block representation.

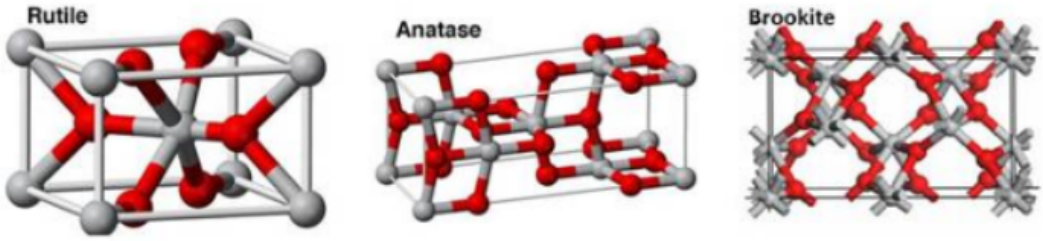

Figure 1.1: Three major phases of TiO_2

The key difference between rutile and anatase comes from the connection of its octahedra, where in rutile they share two edges with other octahedral while in anatase they share four edges.

Table 1.1: Properties of rutile and anatase

Property	*Rutile*	*Anatase*
$Crystal\ Structure$	$Tetragonal$	$Tetragonal$
$Space\ Group$	$P4_2/mnm$	$I4_1/mnm$
$Lattice\ Constants(\AA)$	$a = 4.5934,\ c = 2.9585$	$a = 3.784,\ c = 9.516$
$Atoms\ per\ unit\ cell$	6	12
$Phase\ Transformation$	No	$Rutile\ (400 - 1000^oC)$
$Density\ (g/cm^3)$	4.25	3.89
$Melting\ Point(^oC)$	1855	$Turns\ to\ Rutile$
$Permittivity\ (\varepsilon_r)$	$90(c - axis),\ 170(a - axis)$	$38(c - axis),\ -$
$Ti - O\ bond\ length(\AA)$	$1.949(d_{ax}),\ 1.980(d_{eq})$	$1.965(d_{ax}),\ 1.937(d_{eq})$
$Band\ gap\ (eV)$	3.0	3.23
$Reflectance, \%(at\ 400^oC)$	$47 - 50$	$88 - 90$
$UV\ light\ A\ at\ 360nm\ (\%)$	90	67
$\alpha\ (10^{-6}/K)$	7.14	10.2

1.3 Problem statement

Stoichiometric titanium dioxide which has been studied since the 1950s is known to be an insulator whose band gap is 3.0 eV (rutile) and 3.23 eV (anatase). However, most of the available literature revolves to a large extent around rutile phase, thus leaving a big information gap on another important phase, anatase. This is especially on its electronic properties. Similarly, information available on cross band gap transition is still not very enriching.

1.4 Significance of the study

The application of TiO_2 in industry are many as stated in the introduction, provides a great driving force in research of titanium dioxide. Band gap determination of the two phases of TiO_2 by calculating their electronic properties, provide an insight of observed electrical properties of this industrially and technologically important material. This is so since band gap of materials determine most of its properties hence their applicability. The results of this study therefore, which has been done using computer modelling will supplement information already provided by experimentalists. Additionally, this results will provide more information on the anatase phase. Similarly, it will provide salient information about the possible states responsible for the cross band gap transition.

1.5 Objectives

The following are the objectives under investigation in this study:

1. To determine the structural properties of bulk Rutile and Anatase TiO_2.

2. To determine the electronic properties of both bulk Rutile and Anatase TiO_2.

CHAPTER TWO

LITERATURE REVIEW

2.1 Introduction

Titanium dioxide, which is one of the most important transition metal oxide and extensively studied both experimentally and theoretically. Various empirical and first principle methods calculations have predicted important properties that agrees well with experimental results. In this section, some of the applications of TiO_2 such as in photo catalysis, mainly photo catalytic air purification, photo catalytic sterilization, self cleaning surfaces, decomposition of organic compounds, superhydrophilicity, anti-fogging surfaces, solar energy applications and photo catalytic cancer therapy are reviewed [9].

2.2 Material Modelling

Modelling is a fundamental quantitative method for understanding complex systems and phenomena. Important aspects of materials such as transmittance, thermo-chromic, mechanical and electronic properties play important roles in the functionality of these materials but their manufacture cost greatly influences the consumer costs [19]. The objective of computational materials design is to apply the best scientific understanding to facilitate decisions concerning the optimal trade offs that meet intended needs in the convenient time and resource in efficient manner [8].

Computational materials design has gone along way in addressing these problems because of its flexibility to investigate and control the fabrication of materials of modest complexity. Computer aided molecular designs play a major role by providing the significant structural and energetic properties of atoms that built up the materials [16]. In exploiting its potentials, computer modelling and design combines disciplines such as solid state physics (theoretically), statistical mechanics as well as quantum physics and chemistry. A concise understanding of the fundamental concepts, strengths and limitations is important for designers to fully benefit from these computational methods.

Most theoretical calculations use other empirical and semi-empirical methods such as tight binding and Mott-Littleton methods, molecular dynamics (MD), simulations and more theoretically rigorous first principles approaches are the third class which include: Hartree-Fock (HF) methods and density functional theory (DFT) methods. When modelling a material for energy application as for TiO_2, it is more likely that knowledge with good accuracy of one or more of the following properties; electronic band gap, gap level alignment and optical gap comes in handy.

Theoretical and experimental findings of TiO_2, based on their structural, electronic, optical and magnetic properties have been well reported and documented. However, much of the available data is on rutile phase since most crystal growth techniques yields rutile. Additionally, rutile is the most stable form of TiO_2 since it has the simplest structure. The direct band gap reported for rutile is desirable for the semiconductor applications [4].

CHAPTER THREE

COMPUTATIONAL THEORY

3.1 Introduction

Electronic properties calculations, i.e. ground and excited states, are important aspects in material science. However, the fundamental limitation is the theoretical study of these electronic properties. It is therefore necessary to understand the behaviour of materials i.e atoms, molecules and nano-structures. Electrons and nuclei of materials determine most properties of condensed matter. They provide information about bulk, magnetic, electronic and optical properties. However, it is an uphill task in many system theory when solving the Schrödinger equation for a system of m interacting electrons in the external coulomb field created by a collection of atomic nuclei and other external fields. The exact solution can be achieved solely in the case of the uniform electron gas, atoms with a minimal number of electrons and for a few small molecules. A number of structure methods have been developed in the recent past the key ones will be discussed .

3.2 Theories

3.2.1 Many-Body System

The determination of properties of materials from ab-initio studies involves the solution of a quantum many–system interacting problem for atomic nuclei and electron coordinates,

$$\hat{H}\Psi(\{R_i\},\{r_i,\delta_i\}) = E\Psi(\{R_i\},\{r_i,\delta_i\}) \tag{3.1}$$

3.2.2 Born Oppenheimer approximation

Majority of the properties of material science can be determined by investigating interaction of the outermost electrons with relative slow–moving atomic ionic cores, and the

interaction of outermost electrons amongst themselves. [5].

The nucleus and electrons are attracted to each other with the same magnitude of electric charge, thus they exert the force and momentum while exerting the same kind of momentum, the nucleus with a larger mass in comparison to the electrons, will have a relatively small velocity and considered negligible thus, motion of the nucleus is ignored in solving of Schrödinger equation. The electrons are much less massive than nuclei and therefore electrons respond simultaneously to the motion of nuclei. Thus the energy for a given nuclear configuration will be that of the ground state of electrons in that configuration. The equation that should be solved is therefore;

$$\hat{H}\Psi = E\Psi \tag{3.2}$$

where Ψ is the many–system wave function and E is total energy. The simplest version of the many body Hamiltonian $\hat{H}$, is given by,

$$\hat{H} = \sum_i -\frac{\hbar^2}{2M_i}\nabla_i^2 + \frac{1}{2}\sum_{i,j}\frac{Z_i Z_j e^2}{|\mathbf{R}_i - \mathbf{R}_j|} - \sum_k \frac{\hbar^2}{2m_e}\nabla_{rk}^2 + \frac{1}{2}\sum_{k,l}\frac{e^2}{|\mathbf{r}_k - \mathbf{r}_l|} - \sum_{k,l}\frac{Ze^2}{|\mathbf{r}_k - \mathbf{R}_l|}. \tag{3.3}$$

Principally, the equation above may be mathematically calculated to arbitrary accuracy by representing it as a direct product wave function (BOA) and diagonalizing the Hamiltonian. However, the cost of this calculation scales proportionally with the number of electrons in the system and is intractable for all but the smallest of systems.

3.3 Wave Function Based Method

The eigenfunction of a quantum mechanical operator depends on the co-ordinates upon which the operator acts. A Hamiltonian operator, $\hat{H}$ in QM is the quantum mechanical operator corresponding to the total energy (K.E and P.E) of the systems whose particular eigen function operator is the wave function which is a function that describes the

quantity of states of an isolated system of one or more particles.

3.3.1 Hartree Approximation

The importance of the Hartree method is an introduction to the solution of the many-body systems and to the concepts of self-consistency and of the self-consistent field. In equation (3.4) the K.E. and the nucleus–electron interaction terms are sums of single-particle operators. Each of them act on a single electronic co-ordinate. Similarly, electron-electron interaction term is a pair of interaction acting on pair of electrons. The initial ansatz is that the many-body wave function may be written as ,

$$\Psi(r_1, r_2, ..., r_n) = \Psi_1(r_1)\Psi_2(r_2)\Psi_3(r_1).....\Psi_n(r_n) \tag{3.4}$$

from which it follows that the electrons are independent and interact only via the mean–field coulomb potential. This yield one electron Schrödinger equation of the form,

$$\frac{\hbar^2}{2m}\nabla^2\psi_1(r) + V(r)\psi_1(r) = \epsilon_1\psi_1(r) \tag{3.5}$$

where V(r) is the potential in which the electron moves, this includes both the nuclear electron interaction.

$$V_{nucleus}(r) = -Ze^2\sum_R \frac{1}{|\mathbf{r} - \mathbf{R}|} \tag{3.6}$$

and the mean field arising from the N-1 other electrons. Other electrons are smeared out into a smooth negative charge density ρ(r') leading to a potential of the forms

$$V_{nucleus}(r) = -e\int dx^{'}\rho(r^{'})\frac{1}{|\mathbf{r} - \mathbf{r}^{'}|} \tag{3.7}$$

where, $\rho(r) = \sum_i |\psi(r)|^2$.

Although these Hartree equations are numerically tractable via self–consistent field methods, the approximation fails to capture elements of the essential physics i.e the Pauli exclusion principle which demand that the many–body wave function be antisymmetric with respect to interchange of any two electron co-ordinates. This exchange condition can be satisfied by forming a slatter determinant of single particle orbitals.

3.3.2 Hatree–Fock Approximation

The Hartree–Fock (HF) methods treats electron interactions at a mean field level, with the Hartree and exchange interactions. The simple product of the wave functions in eq. 3.4 does not satisfy the principle of indistinguishability. This does not satisfy antisymmetry, which states that a fermion wave function changes sign under odd permutations of the electronic variable.

3.4 Density Functional Theory

Due to insufficient predictions of chemical bonds and molecular properties met by HF approximation and the high numerical price of wave function approaches, it is important to seek alternative methods that needs to represent the many–body electronic wave function. DFT is one of the most frequently used, computational tools for studying and predicting the properties of materials. Being a ground-state theory, it emphasizes on charge density as the relevant physical quantity. DFT has successfully described structural and electronic properties in most of the materials. For these reasons DFT has become a useful tool in first–principle calculations focused at describing and predicting the properties of molecular and condensed matter systems. Another advantage of DFT is that it can be used in the study of both periodic and non-periodic systems of infinite sizes [14]. Despite recent improvements there are shortcomings in using density functional theory to properly describe intermolecular interactions especially dispersion, charge transfer excitations, transitional states, global potential energy surfaces, dopant interactions and some other strongly correlated system, and in calculations of the band

gap (underestimation of the band gap) and ferro magnetism in semiconductors.

3.4.1 The Hohenberg-Kohn Theorem

DFT is made possible by the existence of simple theorem put forth by Hohenberg and Kohn in 1964. H-K, using the first theorem proved that for a system of N interacting particles in an external potential, $V_{ext}(r)$ the density is uniquely determined i.e the external potential is a unique functional of the density. Variational principle states that no wave function can give an energy that is less the energy of $V_{ext}(r)$ for $\hat{H}_{ext}(\vec{r})$ and by assuming the ground state is non-degenerate then;

$$n(r) = N \int |\psi(r_1, r_2, ..., r_N|^2 dr_1 dr_2 .....dr_N \tag{3.8}$$

where, ψ is the ground state wave function. The result of the H-K theorem is that ground-state energy, E, is uniquely determined by the ground-state charge density,

$$E[n(r)] = F[n(r)] + \int n(r) V_{ext}(r) dr \tag{3.9}$$

where the internal energy F[n(r)] is a universal functional of the charge density n(r) and not of V_{ext}(r). In this manner, DFT exactly simplifies the N-body problem to the determination of a three-dimensional function n(r) which minimizes a functional E[N(r)].

3.4.2 Kohn-Sham Equation

In 1965, Kohn and Sham redefined the many body problem in an elaborate and familiar form which paved way to practical applications of DFT. The Kohn–Sham (K-S) equation is the Schrödinger equation of a non-existing system of non-interacting particles that generate the same density as any given system of interacting particles. The Kohn–Sham equation is defined by a local effective (fictitious) external potential in which the non-interacting particles move, typically denoted as $V_s(\vec{r})$ or $V_{eff}(\vec{r})$, called the Kohn–Sham potential. Within the framework of K-S DFT, the intractable many-body problem of interacting electrons in a static external potential is reduced to

a tractable problem of non-interacting electrons moving in an effective potential. The effective potential includes the external potential and the effects of the Coulomb interaction between the electrons, i.e the exchange and correlations interactions.

3.4.3 Exchange-Correlation Energy

The exchange-correlation energy E(n) is responsible for the change between the exact ground state energy and the energy calculated in HF approximation and using the non-interacting kinetic energy.

$$E_{xc}(n) = T(n) - T_o(n) + U_{xc} \tag{3.10}$$

$T(n)$ and $T_o(n)$ are exact and non interacting kinetic energy functionals respectively, whereas U_{xc} is the interaction of the electrons with their own exchange–correlation hole.

$$E_{xc}[n(r)] = \frac{1}{2} \iint dr dr' \, \frac{[n(r) n_{xc}(r, r')]}{|r - r'|} \tag{3.11}$$

Approximations are sought for $E'_{xc}(n)$ which though it contains also contributions from the kinetic energy, it is usually just called Exchange-correlation functional written as $E_{xc}(n)$. The following subsections explain some typical approximations for the exchange correlation functional that are commonly employed in practical DFT codes.

3.4.3.1 Local Density Approximation (LDA)

LDA revolves around the idea of uniform electron gas. LDA forms the basis of all approximate exchange-correlation functionals. It makes an assumption that the exchange correlation energy at a point r is simply equal to the exchange–correlation energy of a uniform gas that has the same density at a point r.

Despite its simplicity, LDA works better in systems where the charge density is rapidly varying. However, it tends to under predict atomic ground state energies and

ionization energies, while over predicting binding energies. It is also known to overly favour high spin state structure. LDA is also known to predict the wrong magnetic structure of iron. Similarly it incorrectly predicts the band gap of semiconductor materials.

3.4.3.2 Local Spin Density Approximation (LSDA)

LSDA is the generalization of the LDA which includes electron spin. Here the exact spin-scaling is known, but for correction, further approximation is employed. A spin polarized system in DFT employs two spin densities $[n_\uparrow]$ and $[n_\downarrow]$,

$$E_{xc}^{LDA}[n_\uparrow, n_\downarrow] = \int \delta r n(r) \epsilon_{ex}(n_\uparrow, n_\downarrow) \tag{3.12}$$

The exact result of the exchange energy is known in terms of the spin unpolarized functional,

$$E_{xc}^{LDA}[n_\uparrow, n_\downarrow] = \frac{1}{2}\{E_x[2n_\uparrow] + E_c[2n_\downarrow]\} \tag{3.13}$$

and the spin-dependence of the correlation energy is approached by introducing the relative spin polarization,

$$\zeta(r) = \frac{[n_\uparrow(r) - n_\downarrow(r)]}{[n_\uparrow(r) + n_\downarrow(r)]} \tag{3.14}$$

3.5 Pseudopotentials

Practical solutions to the self-consistent(SC) Kohn-Sham (KS) equation are subject to a number of approximations, thus various methods are subject to a number of approximations, thus various have been developed to be cost effective i.e. cause a rapid convergence but without compromising the calculation outcome. Ab $initio$ pseudo-potentials method takes into account only valence electrons leaving the deep inner core states and the strong potential binding them to the nuclei making the calculation relatively cheaper

compared to full potential method. It is generally understood that ion cores (deep inner electrons and nuclei) plays a minimal role on the properties of solids, but their proper inclusion into pseudo potentials creates room for sufficient use of plane-K-Points wave basis sets in electronic structures calculation.

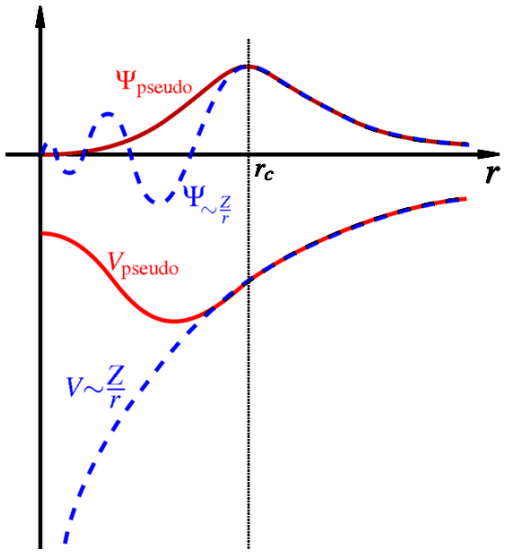

Figure 3.1: Comparison of the wave-function of Coulomb potential of nucleus (blue) to one in pseudo-potential (red). Real and pseudo wave-function and similar potential at certain cut-off radius, r_c

First introduced in 1934 by Hans Hellmann, Pseudo–potentials attempts to replace the complicated effects of the motion of the ion core thus the Schrödinger equation is modified with an effective potential term instead of the Coulomb potential. Pseudo-potentials simply tend to mimic the behaviour of the ion cores of an atom, thus the core states are eliminated and the valence electrons are described by pseudo-wave function with significant fewer nodes.

Although the general ideas behind pseudo-potential approach are similar, several procedures are applied in the construction of these pseudo potential leading to existence of several types of pseudo potentials. Norm-Conserving (NC) and ultra–soft(US) forms the most common forms of pseudo-potentials used in plane-wave electronic structure codes and allows a basis-set with significantly lower cut-off to be used to describe the electron wave function and so allows proper numerical convergence with reasonable computing resources.

Projector augmented wave (PAW) pseudo-potential (PP) first proposed by Peter E. Bloch in 1994, is a method for reformulating an ordinary Kohn-Sham problem with numerically inconvenient behaviour into more computationally digestible form, which involves a different Kohn-Sham problem plus certain corrections. It is a unique way of determining the electron structure of materials since it describes well the nodal behaviour of valence electrons wave function and at the same time allowing the inclusion of the upper core states into the SC interaction procedures. It is a generalization of the PP and linear augmented–plane–wave (LAPW) methods, and allows for DFT calculations to be performed with greater computational efficiency. In this study, norm-conserving pseudo-potentials were used to represent the inner core electrons and the nuclei.

CHAPTER FOUR

METHODOLOGY

4.1 Introduction

The DFT calculations were done within the plane wave basis pseudo-potential approach as performed in the quantum ESPRESSO (QE) code, which is multi-purpose, multi-platform software for first principle calculations for periodic and non-periodic condensed matter systems.

DFT is a technique used commonly to study important properties of materials accurately using a computational method [17]. In this study bulk and electronic properties of TiO_2 (rutile) and TiO_2 (anatase) have been studied using ab-$initio$ pseudo-potential plane wave method within the DFT. Norm conserving pseudo-potentials were used to model the core-valence interactions for bulk calculations.

4.2 K-Point Optimization

The K-points were optimized using the experimental lattice parameter. The K.E cut off was set at 80 Ry for both rutile and anatase an average value not to make the calculations computationally expensive. The special k-mesh points were generated using the Monkhorst-pack scheme that ensures that the irreducible part of the Brillouin zone (IBZ) is integrated over a mesh of $(2 \times 2 \times 2)$ to a dense one of $(12 \times 12 \times 12)$. The dense mesh was required since transition metals like titanium are known to require large k-points grids.

The values of minimum energies obtained with respect to the corresponding k-point grids were plotted for both rutile and anatase phases of TiO_2 (see appendix A, figures 6.1 and 6.5). A $(6 \times 6 \times 6)$ and $(6 \times 6 \times 8)$ mesh of Monkhorst-pack special k-points was selected for rutile and anatase, respectively, since the structures were well converged at this k-points mesh. The k-point were used for all calculations to ensure their accuracy in this study. Figures 4.1 show the k-path that was used for both rutile and anatase phases

of TiO_2.

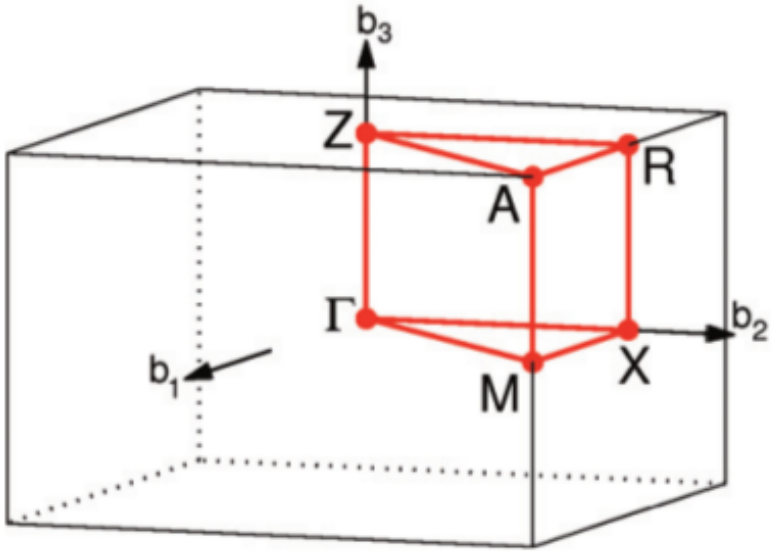

Figure 4.1: High Symmetry Points used in this study.

4.3 Plane Wave Energy Cut-off Optimization

The converged k-point grid was used to calculate the plane wave cutoff energies (Ecut). In this study k-points mesh and lattice parameters were set at their optimized values throughout the calculations. The cutoff energy was varied between 20 Ry and 200 Ry for both rutile, and anatase, (see figures 6.2 and 6.6). The optimized cutoff energy for both rutile and anatase was 80 Ry. Bulk properties were calculated after optimizing k-points and the cut-off energy.

4.4 Modelled and Relaxed Rutile and Anatase TiO_2

Bulk properties of TiO_2 were studied to understand its most basic properties. This was in line with the intention to study the bond lengths, formation energies, band gaps and other properties of interest. Bulk titanium dioxide has the tetragonal structure for rutile and anatase which is specified by a lattice parameter a and the ratio $\frac{c}{a}$ of the vertical axis to one of the horizontal axis. Rutile TiO_2 has tetragonal symmetry and is in space group D_{4h}^{14} -$P4_2/mnm$. Anatase has tetragonal symmetry and is in space group D_{4h}^{19} -$I4_1/mnm$.

Starting from basics of energetics, every system tries to be in a state of minimum energy (ground state), which is obtained by minimizing equation 3.12 to self consistency w.r.t a set of orbitals ψ_i, and to an accuracy of 10^{-8} Ry.

4.5 Structural Optimization

The choice of pseudopotential cut-off energy (E_{cut}) for the plane wave basis and k-points for the Brillouin zone (BZ) are the two most important factors that determine the quality of the numerical calculations. Reliable results can only be obtained if accurate plane wave cut-offs and dense /c-points are used. (E_{cut}) purely depends on the chemical elements used in the calculations. In this study structural optimization was done using convergence tests for k-point mesh and the total energy cut-off. Structural parameters for both rutile and anatase phases of TiO_2 were optimized by relaxing the atoms in x, y and z directions until the systems achieved the minimum energy positions as per the set convergence criteria. The relaxed atomic positions were then used to optimize both the plane wave energy cut-off and the k-point grid. Optimal values of the plane wave cut-off energy and the k-points were used to minimize the total energy as a function of the cell volume.

The structural properties such as lattice equilibrium constant, bulk modulus B_o and ground state energy E_o were obtained from the total energy and fitted to the equation of state (EoS). The converged k-point mesh was then used to calculate the total cut-off energies (E_{cut}) and volumes (V). The values of minimum energies obtained with respect to the corresponding k-point grids were then plotted for both rutile and anatase. These values of k-points were used in all subsequent calculations.

CHAPTER FIVE

RESULTS AND DISCUSSIONS

This chapter presents the findings that were obtained from this study i.e. structural findings, electronic properties, and their respective discussions.

5.1 Structural Optimization

The table 5.1 below give the calculated lattice constants of tetragonal rutile phase of TiO_2. The details of optimization are given in Appendix A. The values are compared with those in literature obtained using different theoretical and experiment approaches.

Table 5.1: Calculated DFT-LDA Lattice parameters for perfect rutile TiO_2, compared with experimental values.

Property	Calculated	Exp Value	Theory	Theory	% dev	Ref
Cell Vol (Å)^3	63.026	62.434	64.840	62.220	+0.948	
a_o (Å)	4.630	4.594	4.653	4.584	+0.784	[1, 11, 12]
$\frac{c}{a}$	0.635	0.644	0.637	0.637	-1.400	
B_o(GPa)	214.0	216.0	209.3	226.7	-0.926	

Table 5.2: Calculated DFT-LDA Lattice parameters for perfect anatase TiO_2, compared with experimental values.

Property	Calculated	Exp Value	Theory	Theory	% dev	Ref
Cell Vol (Å)^3	140.87	136.24	139.84	138.27	+3.30	
a_o (Å)	3.789	3.784	3.763	3.785	+1.32	[3, 20]
$\frac{c}{a}$	2.601	2.515	2.618	2.550	+3.42	
B_o(GPa)	176.2	179.0	172.11	173.4	-2.23	

The values in tables 5.1 and 5.2 show clearly that there is a close relation between calculated and experimental values for both phases (rutile and anatase). The cell volumes were found to very close to the experimental value. On the other hand, the calculated bulk properties of both rutile and anatase were found to be in agreement with those of other theoretical studies and this confirms the results of this study.

Table 5.3: Calculated DFT-LDA bond lengths and angles for pristine rutile and anatase titanium dioxide

Phase Type	Rutile				Anatase			
	Ti-O (Å)		Bond Angles (^{o})		Ti-O (Å)		Bond Angles (^{o})	
Pristine	1.9590_{Ax}	2.0060_{Eq}	$99.95_{Ti-O-Ti}$	131.94_{O-Ti-O}	1.9563_{Ax}	2.0502_{Eq}	$103.81_{Ti-O-Ti}$	152.39_{O-Ti-O}
Exp. Value	1.9820_{Ax}	1.9470_{Eq}	$98.93_{Ti-O-Ti}$	130.01_{O-Ti-O}	1.9650_{Ax}	1.9370_{Eq}	$99.93_{Ti-O-Ti}$	$131.04_{Ti-O-Ti}$

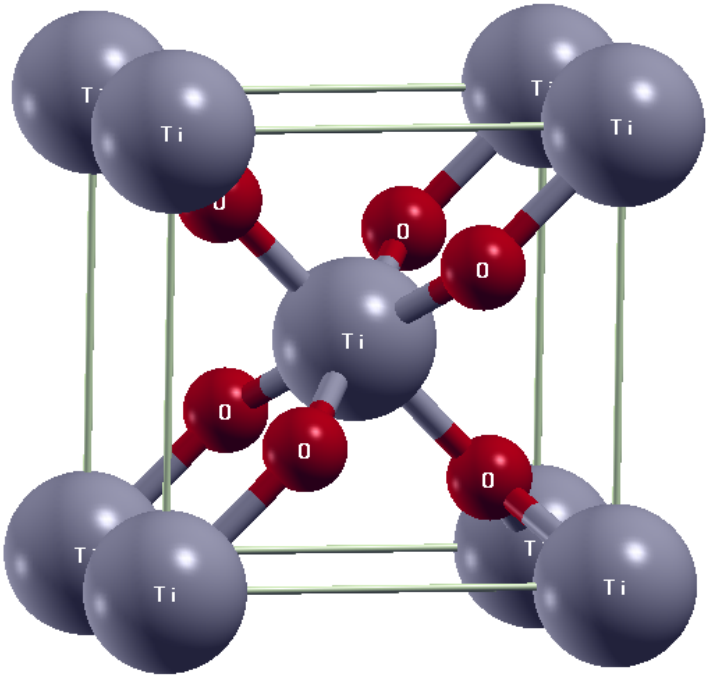

Figure 5.1: Optimized Rutile TiO_2 unit cell.

Table 5.3 gives calculated bond lengths and angles for both rutile and anatase. The values obtained in this study are ground-state results and do not differ much from the experimental results obtained at room temperature because TiO_2 is a solid and a small change in temperature do not affect the structure of solids significantly because their atoms are closely packed. The obtained bond lengths are in agreement with experimental values and other theoretical works.

Looking at table 5.3, d_ax reduces by 2.5% while d_eq increases by also 2.5% that is for rutile after optimization (relax) when compared to unrelaxed system. For anatase TiO_2, the decrease in d_eq is larger than the increase observed in d_ax. The shortening of bond implies strengthening of the bonds due to relaxation. If we compare these findings with the experimental values in table 5.3, for rutile, d_ax was less by 1.14%, while d_eq was more by 2.9%. In the case of anatase, d_eq was underestimated by 1.15% and the d_eq was more (overestimated) by 5.9%.

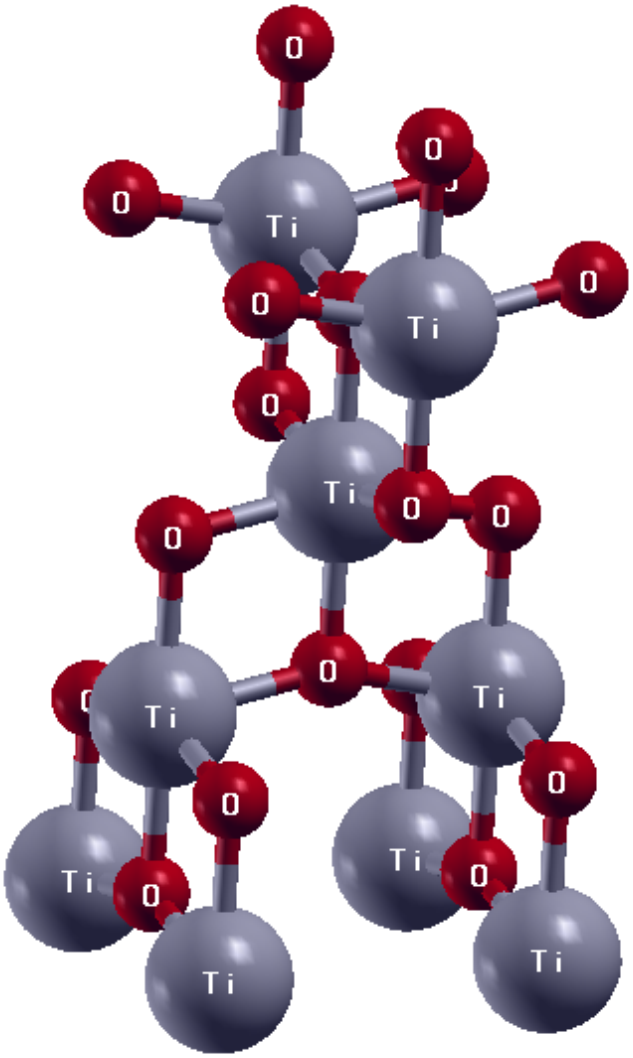

Figure 5.2: Optimized Anatase TiO_2 unit cell.

5.2 Electronic Properties

5.2.1 Band Structure for Perfect Bulk Rutile Crystal

The figure 5.3 below gives the calculated band structure and density of states (DOS) of bulk rutile TiO_2 while the projected density of states (PDOS) are shown in figure 5.4. The electronic band structure was obtained along the high symmetry path Γ – X – M – Γ – Z – R – A – Z – R – A as indicated in figure 5.3. The plot shows a direct band gap of 2.09 eV, at Γ, which is the underestimated when compared with the experimental value of 3.0 eV. A wide valence bands width (VB) of 5.9 eV was calculated and a narrow conduction bandwidth (CB) of 1.65 eV was obtained. These results compares well with other theoretical calculations where valence and conduction band-widths of 5.62 eV were calculated. The value of the valence bandwidth was also in agreement with experimental VB value of 5.4 eV.

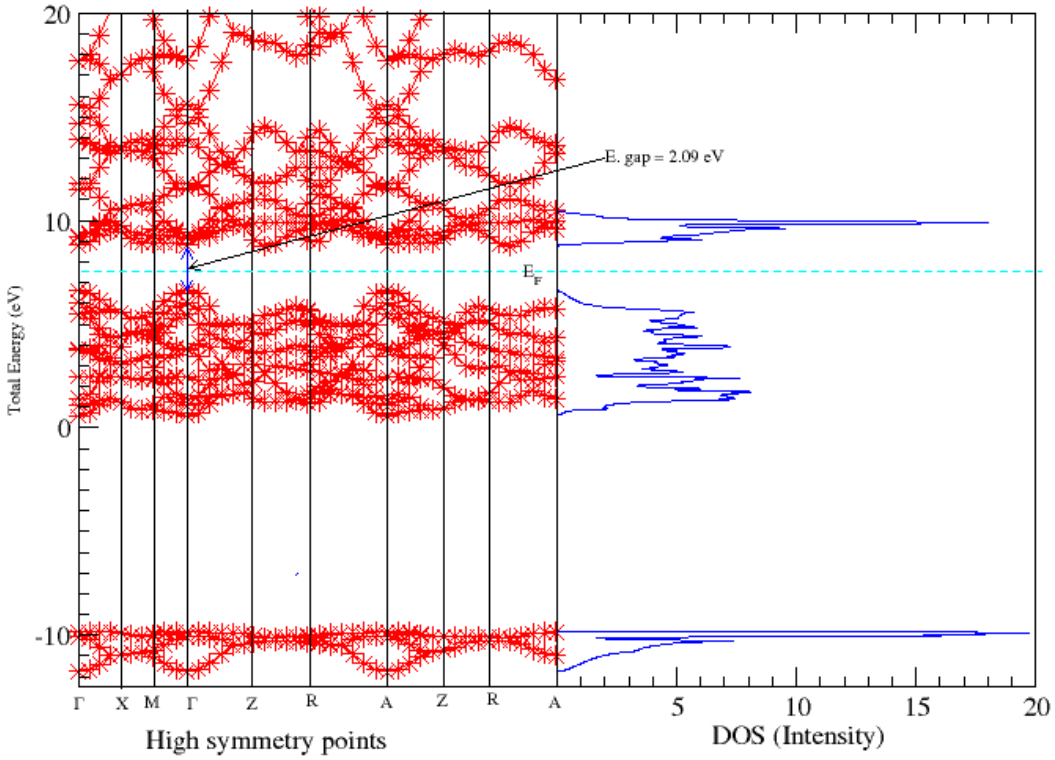

Figure 5.3: Band Structure & DOS for Rutile TiO_2.

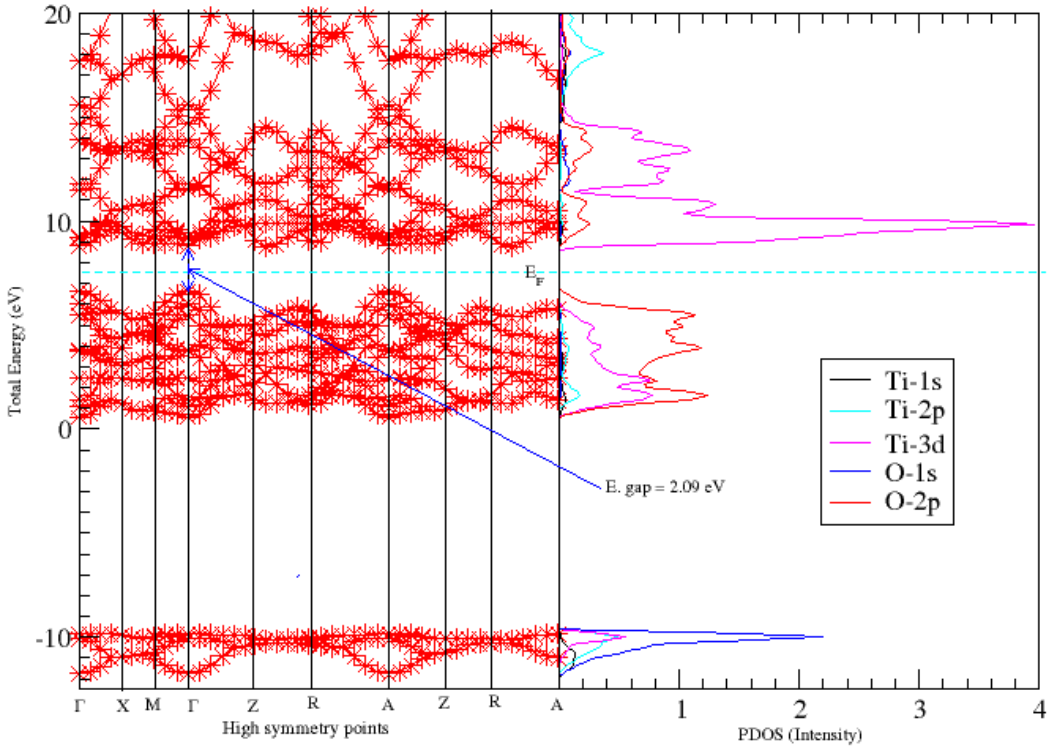

Figure 5.4: Band Structure & PDOS for Rutile TiO_2.

From the graph 5.4 of the projected density of states, it is observed that the valence band was dominated by, Ti-2p, Ti-3d and O-2p states while the conduction band was dominated mainly of Ti-3d and O-2p states, an indication that across band gap transition involves O-2p and Ti-3d orbitals in rutile TiO_2. These hybridized Ti-3d and O-2p states are responsible for the strong bonding observed in rutile. The states at high binding energies were mainly Ti-1s and O-1s.

5.2.2 Band Structure for Perfect Bulk Anatase Crystal

The electronic band structure and density of states of bulk anatase is shown in fig 5.5 while the PDOS are shown in 5.6. The band structure was obtained along the high symmetry path Γ – X – R – Z – M – A – Z. The plot shows an indirect band gap of 2.48 eV along Γ – M which is underestimated when compared with the experimental value of 3.23 eV. This underestimation is attributed to the approximations made in the DFT formalism and can be corrected by using hybrid pseudo-potentials, GW method of DFT+U approaches.

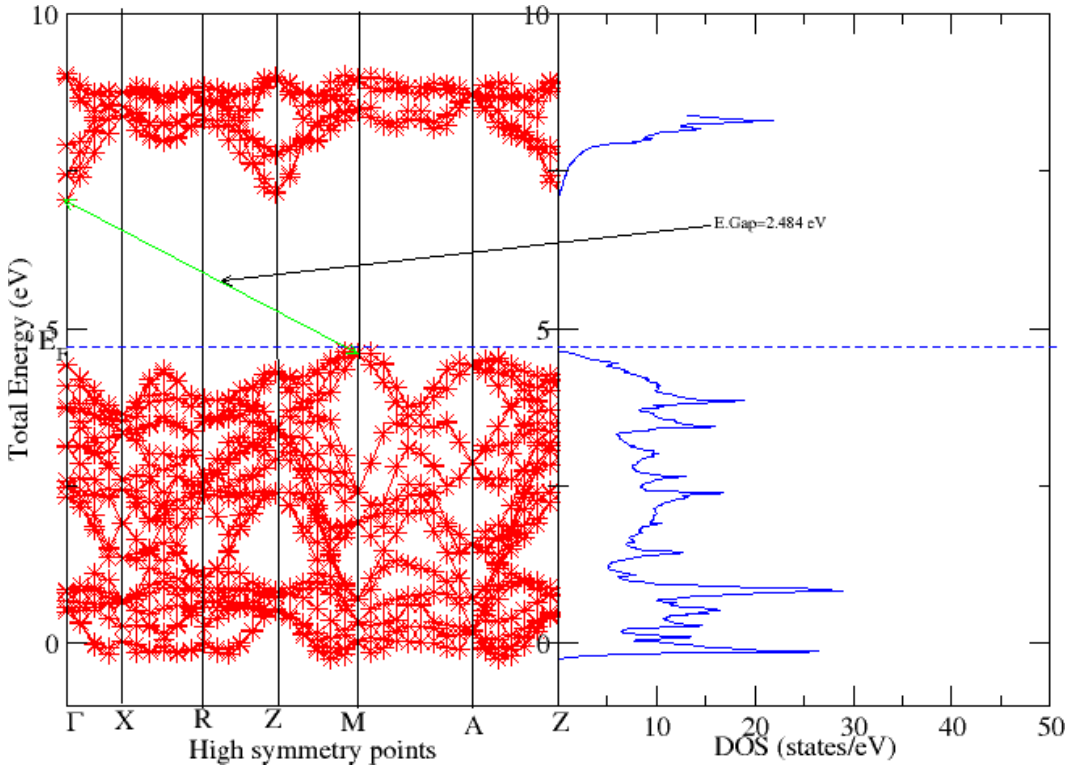

Figure 5.5: Band Structure & DOS for Anatase TiO_2.

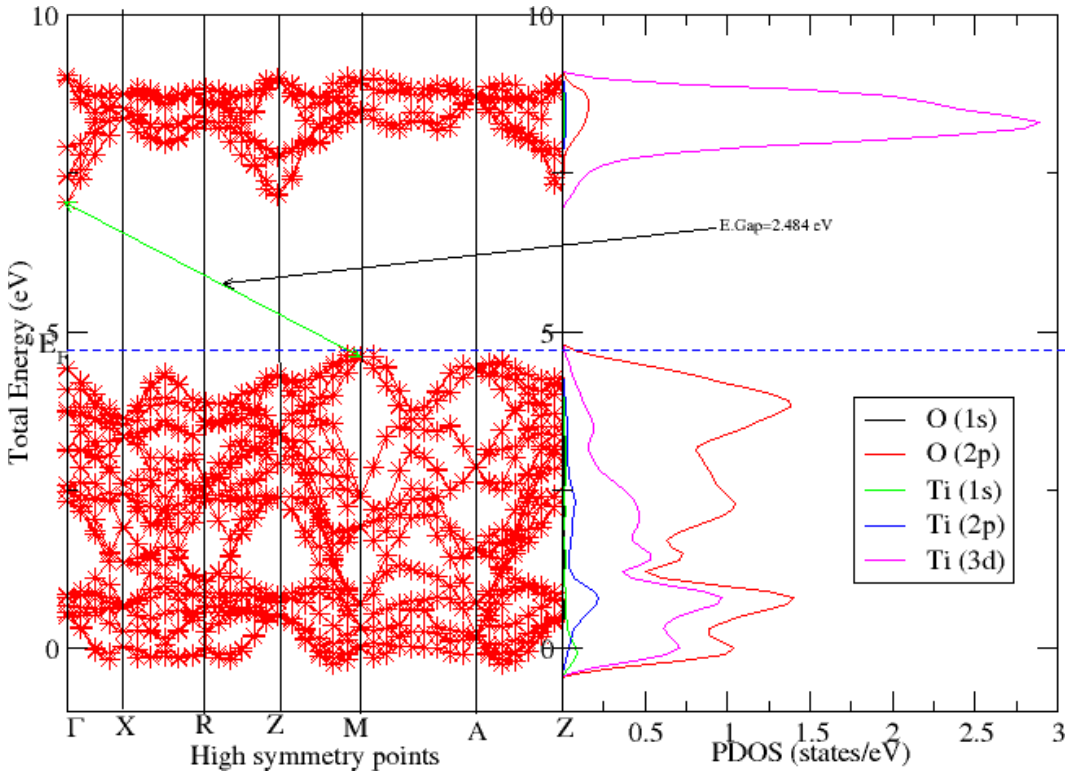

Figure 5.6: Band Structure & PDOS for Anatase TiO_2.

The number of bands of anatase phase of TiO_2 are more than those of rutile phase. Anatase phase was found to have a valence bandwidth of 4.70 eV while the conduction band was narrower with a width of 2.1 eV. The experimental value for valence bandwidth for anatase is 4.75 eV which agrees with the findings of this study. From the projected density of the states of anatase, it was observed that the valence band was dominated by O-(2p) and a little hybridization by Ti-(3d) while, the conduction band was dominated by Ti-(3d) and a little hybridyzation by O-2p states. This is a clear indication that across band gap transition involves both O-2p and Ti-3d orbitals in anatase TiO_2. Similarly, there is an indication that states at high binding energies were mainly Ti-(1s) and O-(1s).

CHAPTER SIX

Conclusions and Recommendations

6.1 Conclusion

Results of first principle studies of the structural and electronic properties in both anatase and rutile phases of titanium dioxide have been investigated in this study using Quantum ESPRESSO code applying norm-conserving pseudo-potentials. The results have been compared with experimental results where available. For ground state properties, a number of important electronic parameters that is band gaps and density of states have been obtained. Except for the band gap values the ground state properties for the two phases are close to experimental values. The rutile structure was found to have a narrow band gap of 2.09 eV while anatase had an indirect band gap of 2.48 eV. The calculated results i.e lattice constant and bulk modulus were found to be consistent with experimental findings and comparatively in good agreement with theoretical predictions. The present calculation has been based on the density functional theory which is strictly valid for ground state. The underestimation of band gaps for semiconductors and insulators is because, a single exchange-correlation potential is inadequate for an insulating system where the exchange-correlation potential is likely to be discontinuous across the gap.

6.2 Recommendation

This study has dealt with only structural and electronic properties of Titanium dioxide. There is need to study the optical properties of the same material since it gives a band gap which is closer to the experimental value.

Bibliography

[1] Batzill, M., Katsiev, K., Gaspar, D. J., and Diebold, U. (2002). Variations of the local electronic surface properties of TiO_2 (110) induced by intrinsic and extrinsic defects. *Physical Review B*, 66(23):235401.

[2] Brune, M., Hagley, E., Dreyer, J., Maitre, X., Maali, A., Wunderlich, C., Raimond, J., and Haroche, S. (1996). Observing the progressive decoherence of the "meter" in a quantum measurement. *Physical Review Letters*, 77(24):4887.

[3] Bryan, J. D., Santangelo, S. A., Keveren, S. C., and Gamelin, D. R. (2005). Activation of high-tc ferromagnetism in co2+: TiO_2 and cr3+: TiO_2 nanorods and nanocrystals by grain boundary defects. *Journal of the American Chemical Society*, 127(44):15568–15574.

[4] Chiodo, L., García-Lastra, J. M., Iacomino, A., Ossicini, S., Zhao, J., Petek, H., and Rubio, A. (2010). Self-energy and excitonic effects in the electronic and optical properties of TiO_2 crystalline phases. *Physical Review B*, 82(4):045207.

[5] Combes, J.-M., Duclos, P., and Seiler, R. (1981). The born-oppenheimer approximation. pages 185–213.

[6] Cox, P. (1996). *The surface science of metal oxides*. Cambridge university press.

[7] Diebold, U. (2003). The surface science of titanium dioxide. *Surface science reports*, 48(5):53–229.

[8] Fahmi, A., Minot, C., Silvi, B., and Causa, M. (1993). Theoretical analysis of the structures of titanium dioxide crystals. *Physical Review B*, 47(18):11717.

[9] Fujishima, A., Rao, T. N., and Tryk, D. A. (2000). Titanium dioxide photocatalysis. *Journal of Photochemistry and Photobiology C: Photochemistry Reviews*, 1(1):1–21.

[10] Glassford, K. M. and Chelikowsky, J. R. (1992). Structural and electronic properties of titanium dioxide. *Physical Review B*, 46(3):1284.

[11] He, J. and Sinnott, S. B. (2005). Ab initio calculations of intrinsic defects in rutile TiO_2. *Journal of the American Ceramic Society*, 88(3):737–741.

[12] Litter, M. and Navio, J. A. (1996). Photocatalytic properties of iron-doped titania semiconductors. *Journal of Photochemistry and Photobiology A: Chemistry*, 98(3):171–181.

[13] Livraghi, S., Paganini, M. C., Giamello, E., Selloni, A., Di Valentin, C., and Pacchioni, G. (2006). Origin of photoactivity of nitrogen-doped titanium dioxide under visible light. *Journal of the American Chemical Society*, 128(49):15666–15671.

[14] Martin, R. M. (2004). *Electronic structure: basic theory and practical methods*. Cambridge university press.

[15] Muscat, J., Swamy, V., and Harrison, N. M. (2002). First-principles calculations of the phase stability of TiO_2. *Physical Review B*, 65(22):224112.

[16] Olson, G. B. (1997). Computational design of hierarchically structured materials. *Science*, 277(5330):1237–1242.

[17] Runge, E. and Gross, E. K. (1984). Density-functional theory for time-dependent systems. *Physical Review Letters*, 52(12):997.

[18] Simons, P. and Dachille, F. (1967). The structure of TiO_2, a high-pressure phase of TiO_2. *Acta Crystallographica*, 23(2):334–336.

[19] Smith, S. J. and Sutcliffe, B. T. (1997). The development of computational chemistry in the united kingdom. *Reviews in Computational Chemistry, Volume 10*, pages 271–316.

[20] Zhang, H., Chen, B., Banfield, J. F., and Waychunas, G. A. (2008). Atomic structure of nanometer-sized amorphous TiO_2. *Physical Review B*, 78(21):214106.

APPENDIX

Convergence Tests of Rutile and Anatase

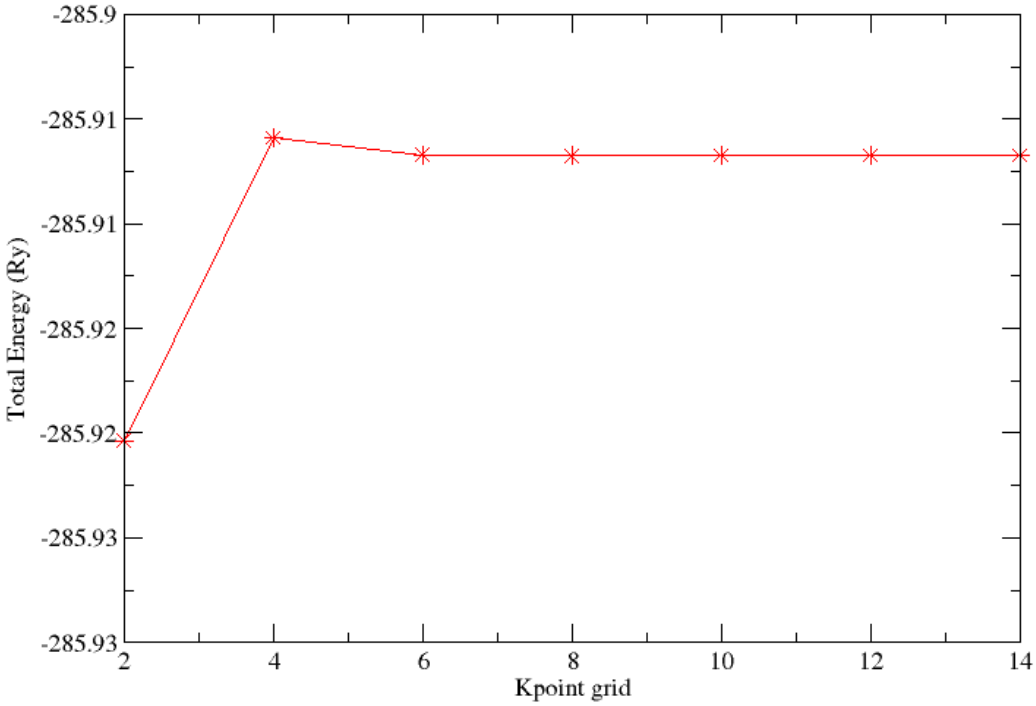

Figure 6.1: Graph of total energy against k-points of bulk anatase phase.

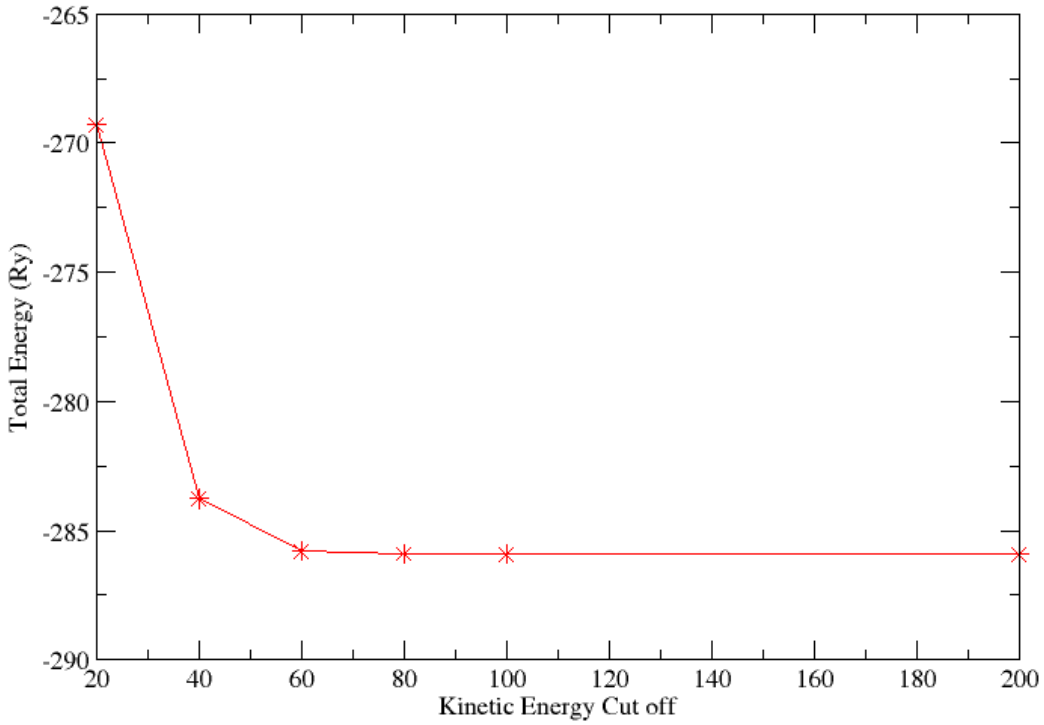

Figure 6.2: Graph of total energy against cut-off energy of bulk anatase phase.

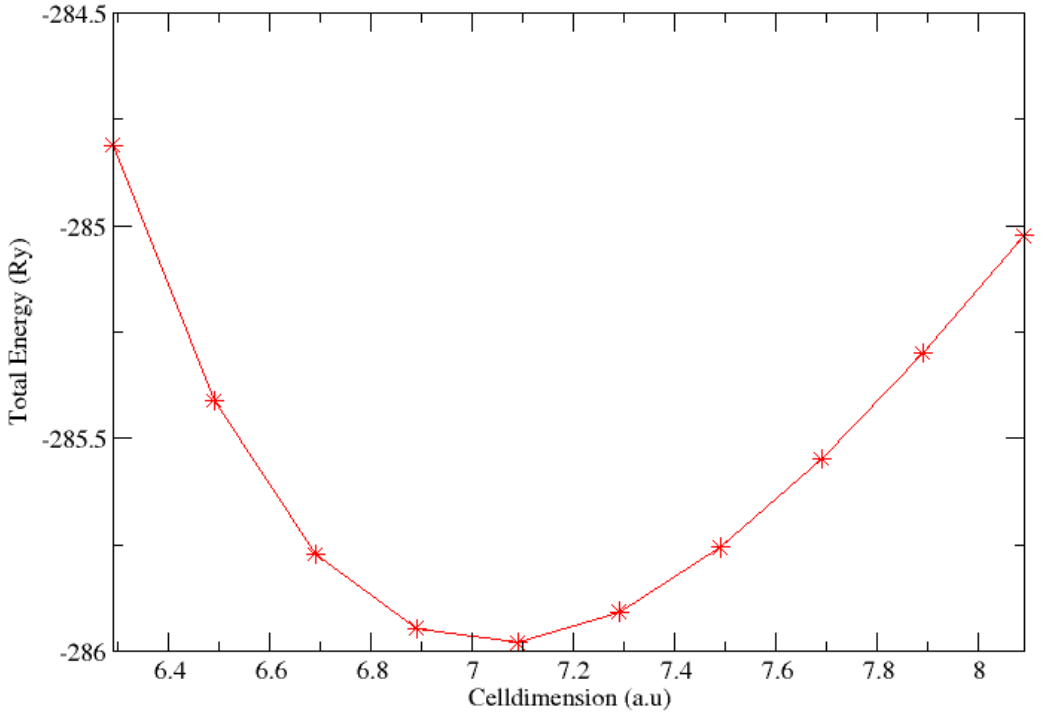

Figure 6.3: Graph of total energy against lattice parameter of bulk anatase phase.

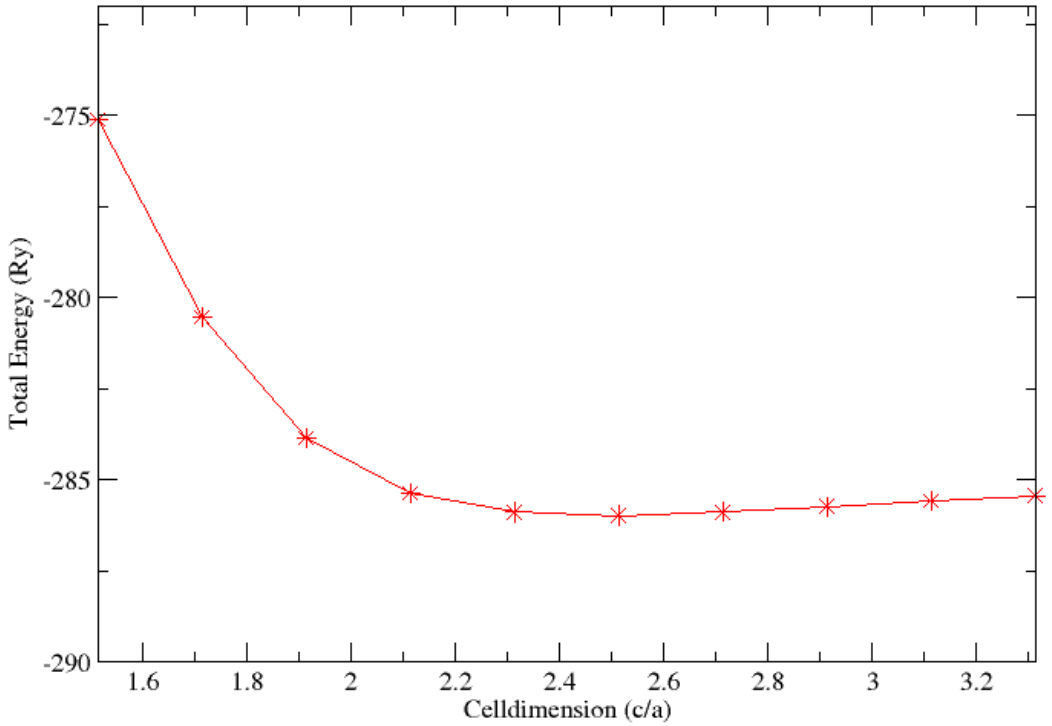

Figure 6.4: Graph of total energy against $\frac{c}{a}$ of bulk anatase phase.

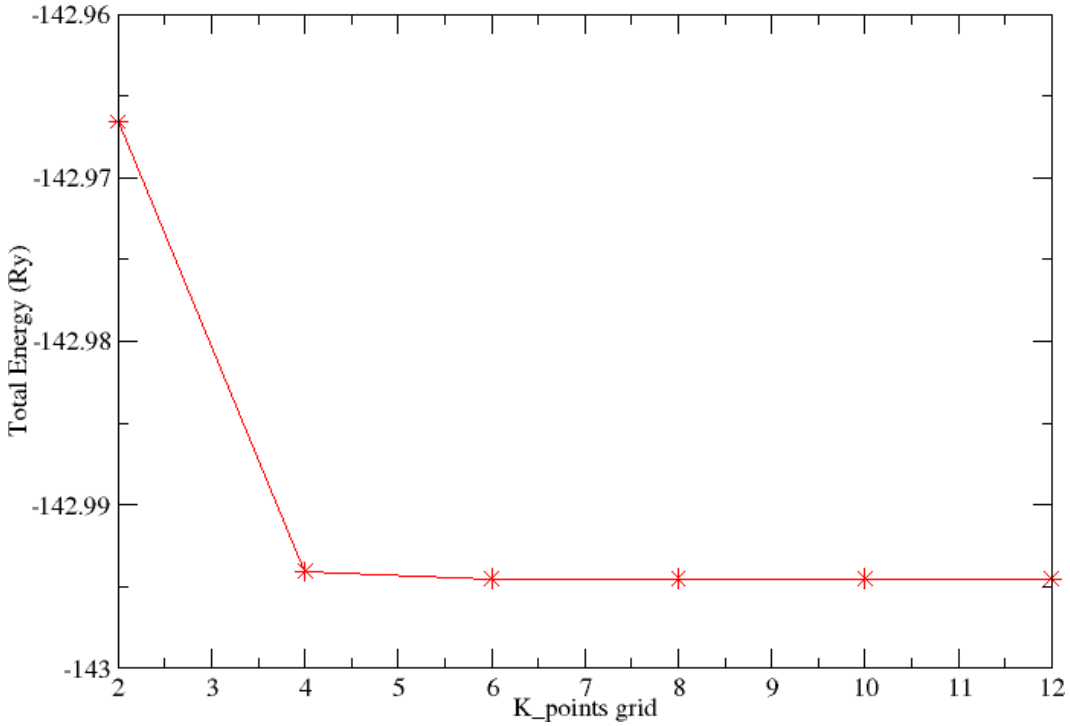

Figure 6.5: Graph of total energy against k-points of bulk rutile phase.

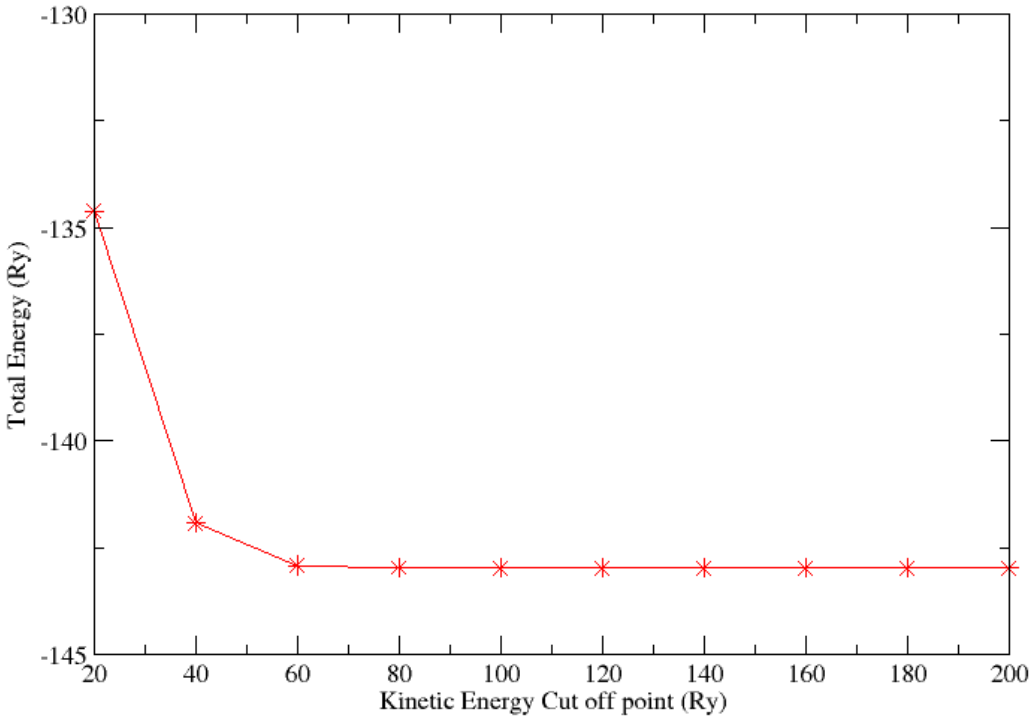

Figure 6.6: Graph of total energy against cut-off energy of bulk rutile phase.

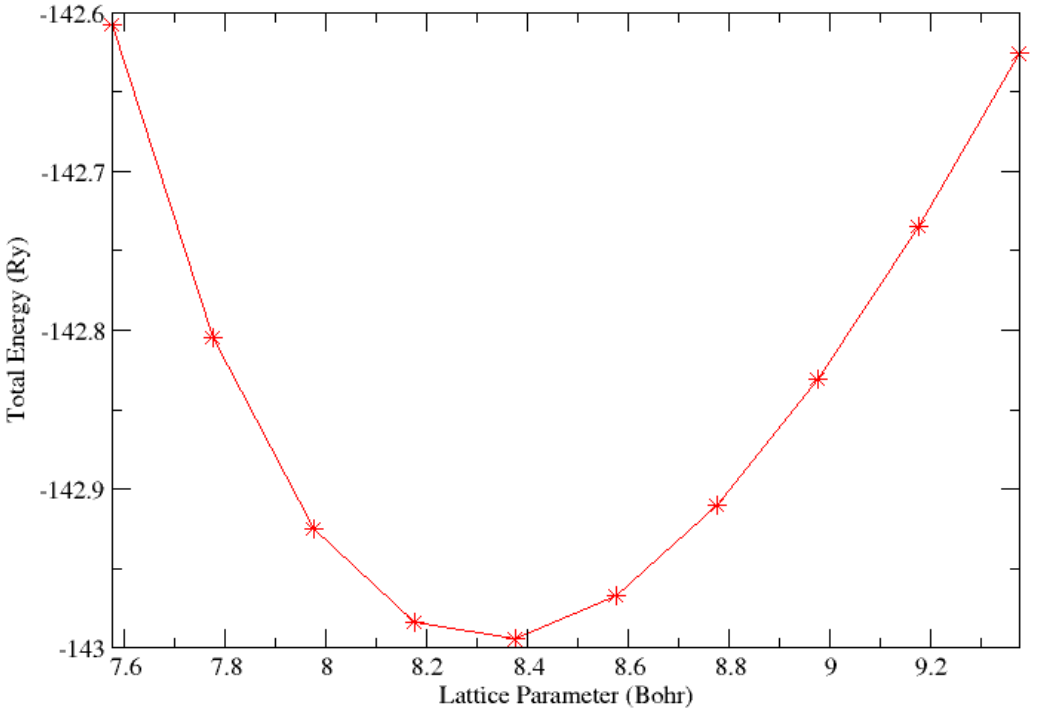

Figure 6.7: Graph of total energy against lattice parameter of bulk rutile phase.

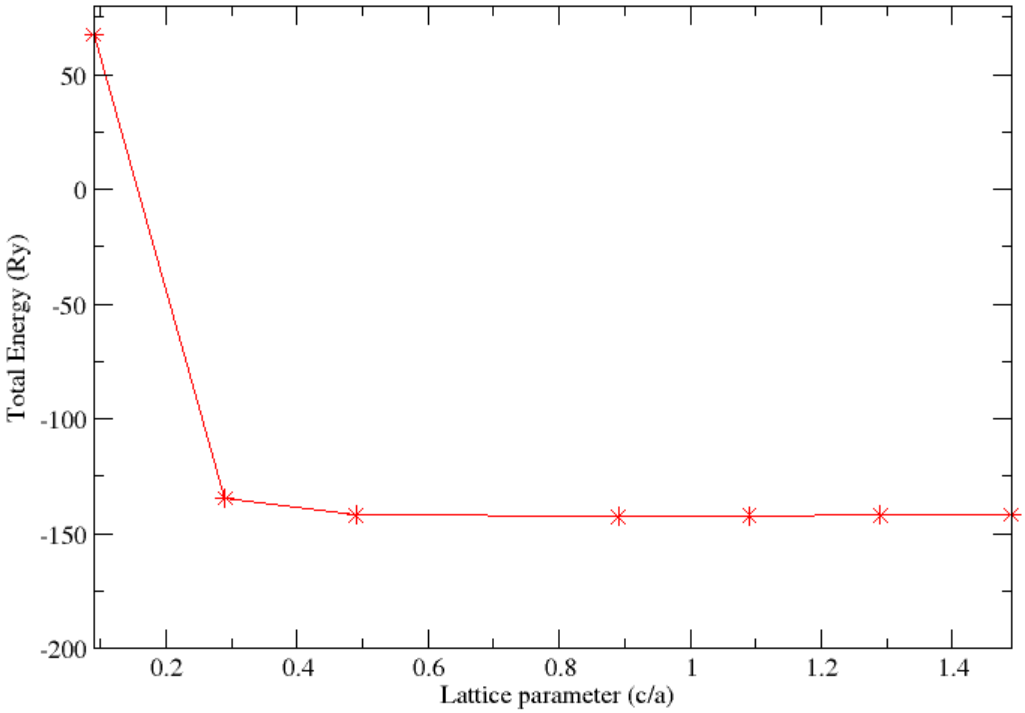

Figure 6.8: Graph of total energy against $\frac{c}{a}$ of bulk rutile phase.

Pseudo-Potentials Used in this Study.

Table 6.1: Pseudo-potentials used for both rutile and anatase TiO_2.

Type of Atom	Pseudo-Potential Type
Titanium	Ti.pbe-mtfhi.UPF
Oxygen	O.pbe-mtfhi.UPF

Titanium

Generated on 10-07-2012 using FH198PP and converted with fhi2upf.x v.5.0.1. The pseudo-potential was generated with a Non-Relativistic Calculation. Its L component and cut-off radius for the Local Potential was 10.0000. The pseudo-potential type is SL.

Table 6.2: Titanium pseudo-potentials.

nl	pn	l	occ	Rcut	Rcut US	E pseu
4s	4	0	2.00	0.000	0.000	0.000000
4p	4	1	2.00	0.000	0.000	0.000000
3d	3	2	0.00	0.000	0.000	0.000000
4f	4	3	0.00	0.000	0.000	0.000000

Ultrasoft Pseudopotential	US
Nonlinear Core Correction	F
PBE Exchange-Correlation Functional	SLA, PW, PBE
Local Potential Cut-off Radius	0.000000000000000E+000
Z Valence	4.0000000000000000
Total Energy	0.00000000000000E+000
Number of Points in Mesh	515
Max Angular Momentum Component	3
Number of Wavefunctions	4
Number of Projectors	3

Oxygen

Generated on 10-07-2012 using FH198PP and converted with fhi2upf.x v.5.0.1. The pseudo-potential was generated with a Scalar Relativistic Calculation. Its L component and cut-off radius for the Local Potential was 20.0000. The pseudo-potential type is SL.

Table 6.3: Oxygen pseudo-potentials.

nl	pn	l	occ	Rcut	Rcut US	E pseu
2s	2	0	2.00	0.000	0.000	0.000000
2p	2	1	4.00	0.000	0.000	0.000000
3d	3	2	0.00	0.000	0.000	0.000000
4f	4	3	0.00	0.000	0.000	0.000000

Ultrasoft Pseudopotential	US
Nonlinear Core Correction	F
PBE Exchange-Correlation Functional	SLA, PW, PBE
Local Potential Cut-off Radius	0.000000000000000E+000
Z Valence	6.0000000000000000
Total Energy	0.00000000000000E+000
Number of Points in Mesh	473
Max Angular Momentum Component	3
Number of Wavefunctions	4
Number of Projectors	3